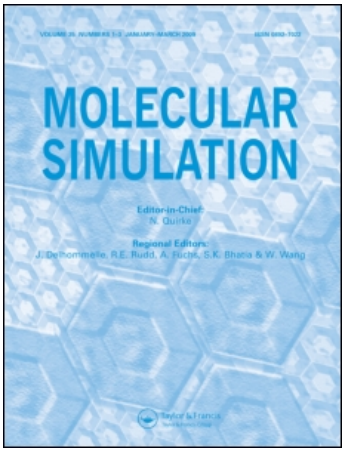

Molecular Simulation
Publication details, including instructions for authors and subscription information:
http://www.informaworld.com/smpp/title~content=t713644482

Polymers of intrinsic microporosity for gas permeation: a molecular simulation study

Weijie Fang[a]; Liling Zhang[a]; Jianwen Jiang[a]
[a] Department of Chemical and Biomolecular Engineering, National University of Singapore, Singapore

Online publication date: 05 November 2010

To cite this Article Fang, Weijie , Zhang, Liling and Jiang, Jianwen(2010) 'Polymers of intrinsic microporosity for gas permeation: a molecular simulation study', Molecular Simulation, 36: 12, 992 — 1003
To link to this Article: DOI: 10.1080/08927022.2010.498828
URL: http://dx.doi.org/10.1080/08927022.2010.498828

Molecular Simulation
Vol. 36, No. 12, October 2010, 992–1003

Taylor & Francis
Taylor & Francis Group

Polymers of intrinsic microporosity for gas permeation: a molecular simulation study

Weijie Fang, Liling Zhang and Jianwen Jiang*

Department of Chemical and Biomolecular Engineering, National University of Singapore, 117576, Singapore

(*Received 7 April 2010; final version received 31 May 2010*)

We report a molecular simulation study for gas permeation in two membranes constructed from polymers of intrinsic microporosity (PIM-1 and PIM-7). With rigid ladder polymer chains, the membranes posses approximately 47.7 and 46.6% fractional free volumes (FFVs) in PIM-1 and PIM-7, respectively. The voids in the membranes have a diameter up to 9 Å and are largely interconnected. The sorption and diffusion of four gases (H_2, O_2, CH_4 and CO_2) were calculated by Monte Carlo and molecular dynamics simulations. The solubility coefficients increase in the order of $H_2 < O_2 < CH_4 < CO_2$, while the diffusion coefficients increase in the following order: $CH_4 < CO_2 < O_2 < H_2$. The simulation results agree well with experimental data, particularly for the solubility coefficients. The solubility and diffusion coefficients correlate well separately with the critical temperatures and effective diameters of gases. These molecular-based correlations can be used in the prediction for other gases. As attributed to the microporous structure, PIM-1 and PIM-7 outperform most glassy polymeric membranes in sorption and diffusion. PIM-1 has larger solubility and diffusion coefficients than PIM-7 because the cyano groups in PIM-1 lead to a stronger affinity and a larger FFV. The simulated solubility, diffusivity and permeation selectivities of CO_2/H_2, CO_2/O_2 and CO_2/CH_4 are consistent with experimental data. The quantitative microscopic understanding of gas permeation in the PIM membranes is useful for the new development of high-performance membranes.

Keywords: polymers of intrinsic microporosity; permeation; molecular simulation

1. Introduction

The development of environmentally clean fuels is of central importance for the sustainable growth of economy. Among many energy alternatives, H_2 and CH_4 are strategically important fuel sources in the foreseeable future. To produce high-quality H_2 and CH_4, the separation of gas mixtures is a key process. A handful of techniques have been proposed for gas separation such as cryogenic distillation, pressure/temperature swing adsorption and membrane permeation. Compared to other methods, polymeric membranes have the advantage of high energy efficiency, low capital cost, large separation capability and ease of scaling-up.

Extensive experimental studies have been reported for gas permeation and separation in polymer membranes, as summarised in several reviews [1–5]. Chung and co-workers [6] reported the synthesis, cross-linking and carbonisation of co-polyimides containing internal acetylene units for gas separation; and proposed a novel synthetic strategy to fine-tune the cavity size and free volume distribution for polyimide membranes via the formation of homogeneous pseudo-interpenetrating polymer networks [7]. Radosz and co-workers [8] measured the transport of CO_2, CH_4 and N_2 in silica-impregnated, brominated poly(phenylene oxide) as a function of silica size and concentration. Ribeiro and Freeman [9] and Yave et al. [10] separately determined the sorption of CO_2 in poly(ethylene oxide) and poly(ethylene oxide)–poly(butylene terephthalate). As an alternative, molecular simulation studies have been reported for gas permeation in polymer membranes. Mark and co-workers [11,12] calculated gas permeabilities in poly(2,6-dimethyl-1,4-phenylene oxide) and elucidated the unusually high permeabilities in poly(dimethylsiloxane). Hofmann and co-workers [13,14] constructed atomistic packing models for glassy polyimides, polysulphone and poly(ether sulphone); and calculated gas solubility and diffusion coefficients. Theodorou and co-workers [15,16] simulated the structural, conformational, dynamics and barrier properties of amorphous poly(ethylene terephthalate) and poly(ethylene isophthalate), and predicted CO_2 sorption in glassy atactic polystyrene. Neyertz et al. [17,18] reported O_2 transport in glassy polyimides with different chain configurations and free-standing polyimide membranes.

In the continuous quest for novel polymeric membranes, a novel class of polymers, namely, polymers of intrinsic microporosity (PIMs) have recently been synthesised [19–21]. PIMs are amorphous, thermally stable and glassy polymers. Remarkably, PIMs have microporous character and are potentially useful for gas separation, hydrogen storage and heterogeneous catalysis. To date, only a few studies have been reported on the preparation and modification of PIMs for gas separation. For instance, two PIM (PIM-1 and PIM-7) cast into membranes were found to have high performance in gas

*Corresponding author. Email: chejj@nus.edu.sg

ISSN 0892-7022 print/ISSN 1029-0435 online

DOI: 10.1080/08927022.2010.498828
http://www.informaworld.com

separation [22,23], and indeed exceed the trade-off between permeability and selectivity proposed by Robeson [24]. Mixed-matrix membranes (MMMs) formed by PIM-1 and silica nanoparticles showed enhancement in gas permeability due to the cavities between organic and inorganic phases [25]. PIM-1-derived membranes with functionalised side groups such as trifluoromethyl, phenylsulphone, carboxyl outperformed the prototypical PIM-1 membrane in gas separation [26–28]. PIM-polyimide copolymers were found to exceed Robeson's upper bound and showed potential for gas separation [29]. An atomistic packing model was built for PIM-1 and the free volume distribution and gas transport in the model membrane were examined [30].

A more detailed study for PIMs is desirable towards the development of next-generation polymeric membranes for high-performance gas separation. In this study, we report a molecular simulation study on the sorption, diffusion and permeation in both PIM-1 and PIM-7 membranes. With the ever increasing computational power, molecular simulation has become increasingly important in polymer sciences. In particular, the microscopic insights from simulation are indispensable in quantitatively elucidating the underlying physics and subsequently to provide guidelines for the intelligent design of new polymer membranes. In section 2, we explain how to construct and characterise the atomistic models for PIM-1 and PIM-7 membranes. The simulation methods are then introduced, including Monte Carlo (MC) and molecular dynamics (MD) simulations to calculate solubility and diffusivity, respectively. In section 3, the free volumes and void distributions are presented for PIM-1 and PIM-7. The solubility, diffusivity and permeability of four industrially important gases (H_2, O_2, CO_2 and CH_4) are reported and compared with available experimental data. In addition, the ideal selectivities of CO_2 with respect to H_2, O_2 and CH_4 are evaluated.

2. Simulation models and methods

2.1 Atomistic models

PIM-1 and PIM-7 were experimentally synthesised from 5,5′,6,6′-tetrahydroxy-3,3,3′,3′-tetramethyl-1,1′-spirobisindane by the polycondensation reaction [19–21]. Figure 1 shows the synthesis processes and structures of PIM-1 and PIM-7. The backbones of PIM-1 and PIM-7 contain aromatic rings that are connected by spiro-centres (i.e. tetrahedral carbon atoms shared by two rings). These unique polymer chains lead to a rigid contorted molecular structure. As a consequence, the atomic packing is not efficient and intrinsic porosity exists in PIM-1 and PIM-7 membranes. The primary difference between PIM-1 and PIM-7 is the presence of cyano (—C≡N) groups in PIM-1. As we shall see below, this causes different fractional free volumes (FFVs), solubility and diffusion coefficients in the two PIMs.

In our study, the polymer chains of PIM-1 and PIM-7 were constructed and terminated by hydrogen atoms rather than by halogen atoms (fluorine and chlorine). Each polymer chain consisted of a number of repeat units (15 for PIM-1 and 10 for PIM-7) arranged in a random torsional angle. Compared to PIM-1, the number of atoms in the repeat unit of PIM-7 is larger; therefore, a shorter PIM-7 chain was constructed in order to have a comparable number of atoms in the two polymer chains. PIM-1 and PIM-7 membranes were built by the *Amorphous Cell* in Materials Studio 4.3 (Accelrys Inc., San Diego, CA, USA) using the scheme of Theodorou and Suter [31]. Each membrane was composed of three polymer chains in a periodic cubic simulation box, with an initial density of $0.1\,g/cm^3$ and a target density of $1.0\,g/cm^3$. Ten configurations were generated and three of them were selected for equilibration by the following subsequent procedures: (1) energy minimisation at zero Kelvin with five million steps; (2) 500 ps NVT-MD simulation at 600 K; (3) 500 ps NPT-MD simulation at 600 K at 1 bar; (4) thermal annealing at 1 bar from 600 to 300 K with a temperature interval of 50 K; (5) 100 ps NPT-MD simulation at 10 bar with a time step of 0.1 fs; and (6) 2000 ps NPT-MD simulation with a time step of 1 fs at 300 K and 1 bar.

The energy minimisation and MD simulations were conducted in DL_POLY [32,33] instead of Materials Studio. For this purpose, an in-house code was developed to convert the structure files created by Materials Studio to DL_POLY. In such a way, the computational time was reduced by one to two orders of magnitude. The polymers were mimicked by the polymer consistent force field (PCFF) [34–37] with bonded and non-bonded terms. The cross-coupling terms were omitted due to the trivial corrections in the present context. The bonded term U_{bonded} consists of

$$\begin{aligned} U_{\text{bonded}} = & \sum_b [k_2^b(b-b_0)^2 + k_3^b(b-b_0)^3 + k_4^b(b-b_0)^4] \\ & + \sum_\theta [k_2^\theta(\theta-\theta_0)^2 + k_3^\theta(\theta-\theta_0)^3 + k_4^\theta(\theta-\theta_0)^4] \\ & + \sum_\phi [k_1^\phi(1-\cos\phi) + k_2^\phi(1-\cos 2\phi) \\ & + k_3^\phi(1-\cos 3\phi)] + \sum_\chi k^\chi(\chi-\chi_0)^2, \end{aligned} \tag{1}$$

where b, θ, ϕ and χ represent bond length, bond angle, dihedral angle or out-of-plane angle formed by pairs, triplets and quadruplets, respectively. The non-bonded term $U_{\text{non-bonded}}$ consists of Lennard-Jones (LJ) and Coulombic potentials:

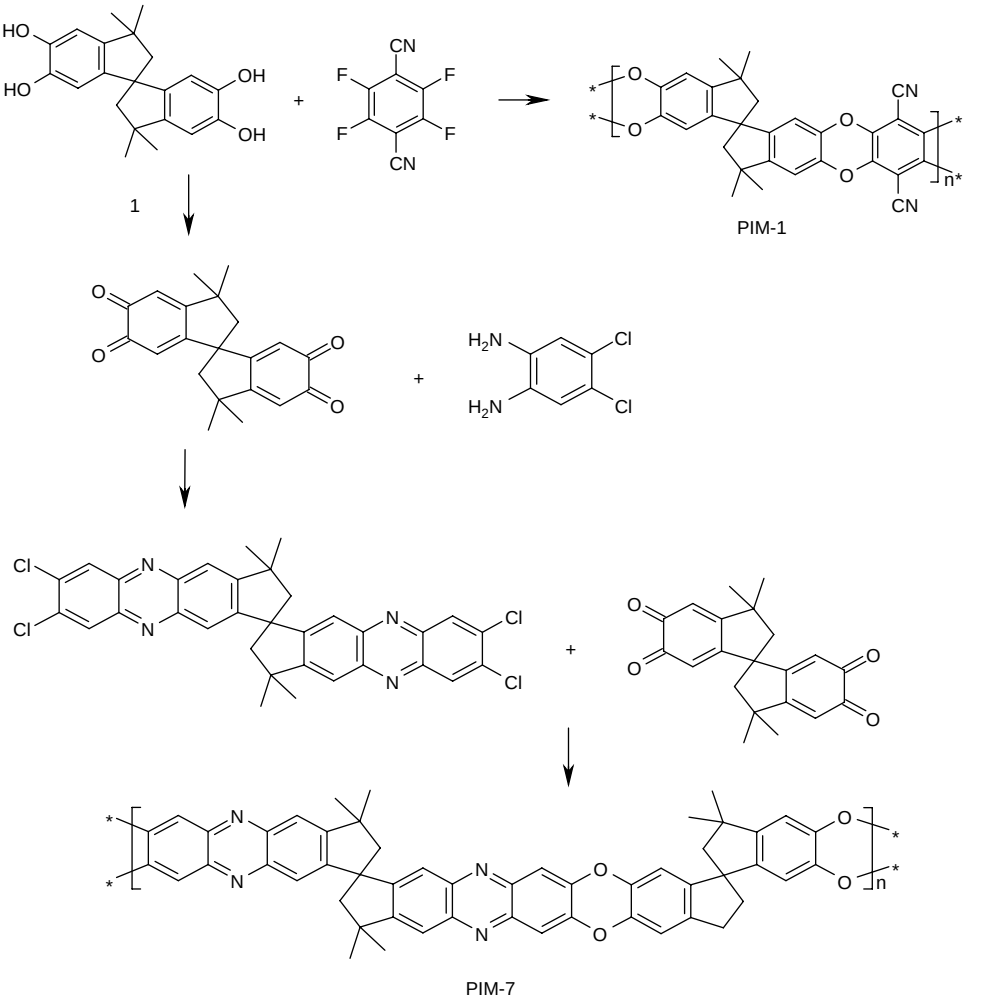

Figure 1. Schematic synthesis processes and structures of PIM-1 and PIM-7.

$$U_{\text{non-bonded}} = \frac{1}{4\pi\varepsilon_0}\sum_{i,j}\frac{q_i q_j}{r_{ij}} + \sum_{i,j}\varepsilon_{ij}\left[2\left(\frac{r_{ij}^0}{r_{ij}}\right)^9 - 3\left(\frac{r_{ij}^0}{r_{ij}}\right)^6\right], \quad (2)$$

where ε_0 is the permittivity of vacuum; q_i is the atomic charge on atom i; r_{ij} is the distance between atoms i and j; ε_{ij} and r_{ij}^0 are the well depth and collision diameter of the LJ potential. The LJ interactions were calculated with a cut-off of 13 Å and the Coulombic interactions were treated by the Ewald sum with a precision of 10^{-5}. The velocity Verlet algorithm was used in the MD simulation. Temperature and pressure were controlled by the Berendsen method [38] with a decay constant of 0.6 ps.

The equilibrated models of PIM-1 and PIM-7 membranes were characterised by solubility parameter, free volume and void distribution. The solubility parameter was evaluated by the cohesive energy of polymer. The free volume and void distribution in a polymer membrane play a crucial role in gas transport. Experimentally, positron annihilation lifetime spectroscopy is commonly used to determine the free volume by measuring the lifetime of positronium [39]. In this study, the free volume and void size distribution were estimated geometrically by MC simulation using an in-house developed code. A probe was randomly inserted into a simulation box and the insertion was considered to be successful if the probe did not overlap with any polymer atom. The ratio of successful insertion to the total number of insertion gave the FFV. The free volume was simply the product of the FFV with the volume of the simulation box. We estimated the total FFV, that is, with the probe radius equal to zero. The void size distribution was estimated by a method previously used for microporous materials [40,41]. In brief, the simulation box was divided into 3D fine grids with a size of approximately 0.1 Å. The void size at a grid was determined as the diameter of the maximum cavity that enclosed the grid and additional had no overlap with any polymer atom.

2.2 Sorption and diffusion

Gas permeation in a polymeric membrane is based on the solution–diffusion mechanism. Specifically, the gas first dissolves at feed side, diffuses through a membrane and finally departs at the product side. With different solubilities and diffusivities in a membrane, gases can be separated. The four gases considered (H_2, O_2, CO_2 and CH_4) were also mimicked by the PCFF [34–37]. At a given pressure p, the solubility c of a gas is governed by the solubility coefficient $S(c,p)$:

$$c = S(c,p)p. \tag{3}$$

In this study, the solubility coefficient was evaluated at infinite dilution and hence $S(c,p)$ was equal to Henry's constant K_H. From statistical mechanics, it is easy to derive

$$K_H = \beta \exp\left(-\beta\mu_{ex}^0\right), \tag{4}$$

where $\beta = 1/k_BT$ is the reciprocal temperature and μ_{ex}^0 is the excess chemical potential at infinite dilution. From the Widom insertion method [42], Equation (4) becomes

$$K_H = \beta \int \exp\left[-\beta u_a(r, \varpi)\right] \mathrm{d}r\, \mathrm{d}\varpi, \tag{5}$$

where $u_a(r, \varpi)$ is the interaction energy between a membrane and a single gas molecule at position r and orientation ϖ.

Diffusion in PIM-1 and PIM-7 was simulated by the MD method. Three gas molecules were inserted into the simulation box of the model membrane. At least half of the box length existed between the gas molecules in order to minimise their interactions. In this regard, the diffusion was examined at infinite dilution. MD simulation was performed in an NVT ensemble for 12 ns. The first 5 ns were used for equilibration and the remaining 7 ns for analysis. Similar to the MD simulation for the equilibration of the polymer membrane, the LJ and Coulombic interactions were also calculated with a cut-off of 13 Å and the Ewald sum. Temperature was controlled by the Berendsen method [38] with a decay constant of 0.6 ps. The mobility of polymer chains and gas molecules was identified by the mean-squared displacement (MSD) defined as

$$\mathrm{MSD}(t) = \frac{1}{N}\sum_{k=1}^{N}\left\langle |r_k(t) - r_k(0)|^2 \right\rangle, \tag{6}$$

where N is the number of polymer or gas molecules, $r_k(t)$ is the position of the molecule k at time t. MSD was calculated from the ensemble average $\langle \ldots \rangle$ of the trajectory. In the calculation, the multiple-origin method was used to improve statistical accuracy.

3. Results and discussion

3.1 Membrane characterisation

Figure 2 shows the typical atomistic models of PIM-1 and PIM-7 membranes after MD equilibration. The backbones of PIM-1 and PIM-7 are rigid due to the considerable amount of aromatic rings; consequently, intramolecular rotation occurs only at the spiro-centres. As discussed below, interconnected voids are formed due to the inefficient packing of the polymer chains. Table 1 lists the predicted properties of PIM-1 and PIM-7 model membranes averaged from three independent runs with different initial configurations. The densities of both the models are close to the experimentally determined values of PIM-1 (1.061–1.092 g/cm^3) [30] and PIM-7 (1.086 g/cm^3) [43]. The deviations between the predicted and experimental densities are 3–4%. This indicates that the PCFF is fairly good in predicting the densities of PIM-1 and PIM-7 membranes. However, further improvement is desired to achieve a better agreement, such as using a more accurate force field. We note that precise pVT properties of a model membrane are critical to its performance.

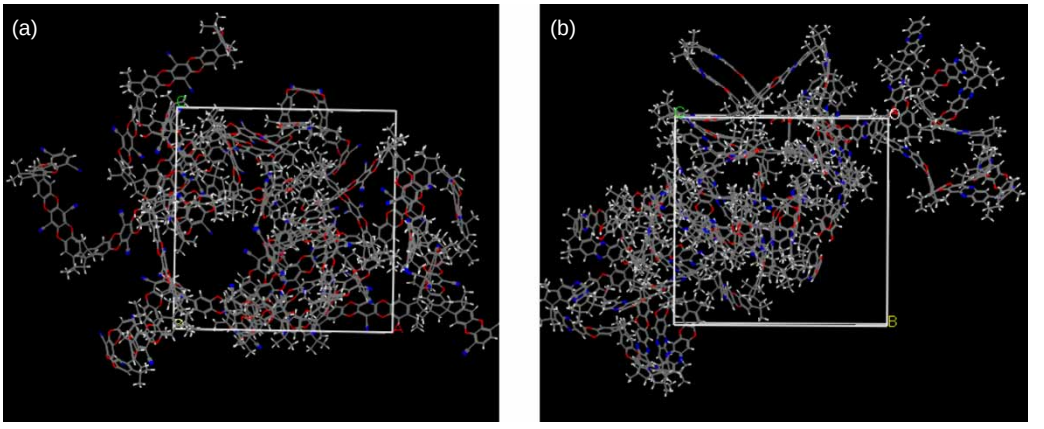

Figure 2. Typical atomistic models of (a) PIM-1 and (b) PIM-7. Colour code: carbon, grey; nitrogen, blue; oxygen, red; hydrogen, white (colour online).

Table 1. PIM-1 and PIM-7 model membranes in this work.

Membrane	PIM-1	PIM-7
Density (g/cm^3)	1.031 ± 0.004	1.041 ± 0.002
CED (J/cm^3)	218.45 ± 6.81	216.97 ± 5.51
Solubility parameter δ (J/cm^3)$^{1/2}$	14.78 ± 0.23	14.73 ± 0.18
Number of atoms	2487	3192
Box length (Å)	32.15	34.96

Solubility parameter is one of the important characteristics of a polymer, which is defined as

$$\delta = \sqrt{\frac{E_{coh}}{V}} = \sqrt{\frac{E_{vac} - E_{bulk}}{V}}, \quad (7)$$

where E_{coh} is the cohesive energy per mole obtained from the energy difference between the molecule in vacuum (E_{vac}) and in amorphous bulk state (E_{bulk}). V is the molar volume and E_{coh}/V is the cohesive energy density (CED). CED can be interpreted as the energy that keeps polymer molecules to stay together. As shown in Table 1, the CED and δ of PIM-1 and PIM-7 are very close, implying that the interactions of PIM-1 and PIM-7 are similar due to their largely similar chain structures.

The voids and their distributions in a polymer membrane govern sorption and diffusion of gas molecules. The FFVs in PIM-1 and PIM-7 were calculated by averaging 100 frames and found to be 47.7 and 46.6%, respectively. These FFVs are substantially larger than in common polyimide membranes (30–38%) [13]. They are also larger than that in silicalite (37%), but smaller than those in metal-organic frameworks (MOFs) and covalent-organic frameworks (COFs) [44,45]. MOFs and COFs are an emerging novel class of hybrid nanoporous materials and have shown high potential in gas storage and separation [46,47]. Figure 3 illustrates the void morphologies in PIM-1 and PIM-7. We observe that the voids are mostly interconnected due to the intrinsic porosity. In other words, there exist continuous voids (holes) in the membranes. This implies that the PIM membranes are zeolite-like from the geometrical point of view. The voids in a membrane vary in size and have different contributions to gas transport. As shown in Figure 4, both PIM-1 and PIM-7 membranes exhibit a wide range of void size distributions with a diameter in the range of 0–9 Å. A comparison between PIM-1 and PIM-7 indicates that PIM-1 has a larger FFV and a slightly higher percentage of voids with a diameter >6.5 Å. This is attributed to the cyano groups in PIM-1, which lead to a steric hindrance and inefficient packing of the PIM-1 membrane. The larger voids contribute predominantly to gas diffusion; consequently, as we will see below that the diffusion coefficients in PIM-1 are generally greater than those in PIM-7.

The mobility of polymer chains in a membrane plays an important role in gas transport. Upon the motion of polymer chains, the voids in the membrane change their size and shape, which would activate or block gas molecules to transport. Figure 5 shows the MSDs of polymer chains in PIM-1 and PIM-7. As can be seen, the mobility of polymer chains is very small due to the stiffness of the polymer chains.

3.2 *Sorption*

Table 2 lists the solubility coefficients of four gases (H_2, O_2, CO_2 and CH_4) in PIM-1 and PIM-7 at 300 K. The simulated results were the averages of three independent runs with different initial configurations. A fairly good agreement is observed between the simulation and the experiment for all the four gases. The predicted solubility coefficients here match with the experiment better than those evaluated by the coarse-grained transition-state theory [30]. Compared to all other polymers reported to date, PIM-1 and PIM-7 show the largest solubility

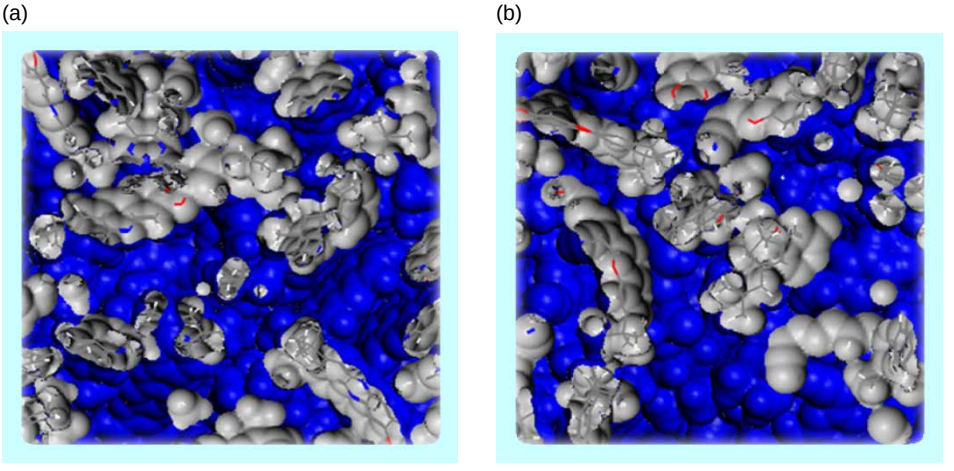

Figure 3. Void morphologies in (a) PIM-1 and (b) PIM-7 as denoted by the blue regions. The grey regions are polymer chains.

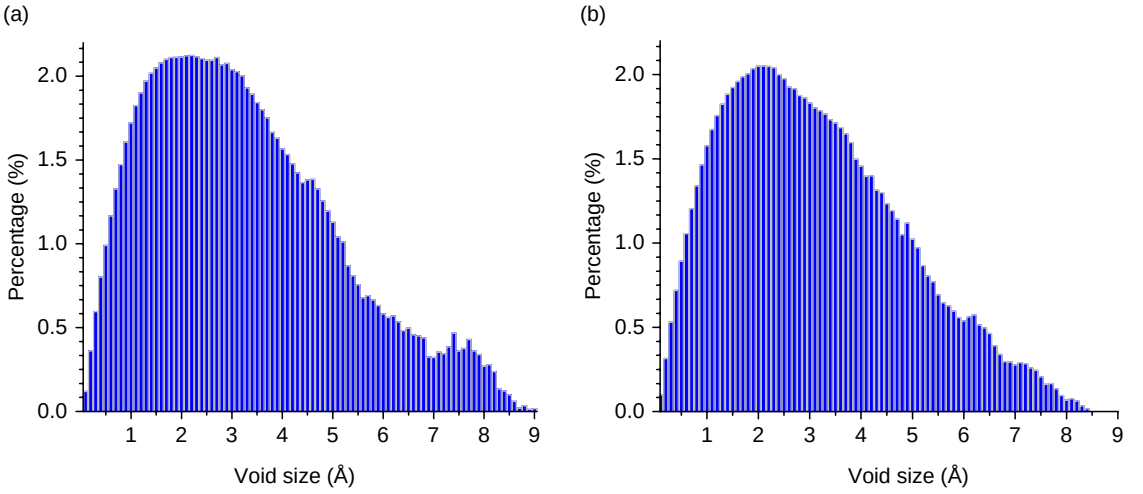

Figure 4. Void size distributions in (a) PIM-1 and (b) PIM-7.

coefficients as a consequence of the presence of microporous structure and polar sorption sites [22,23]. This is unique for these glassy PIMs because large solubility is usually observed in rubbery polymers. The solubility coefficients in PIM-1 appear to be slightly larger than in PIM-7 (particularly in the experimental data). The reason is that PIM-1 contains cyano groups that enhance the affinity for gas molecules. To further elucidate, the structural and energetic properties were calculated for CO_2 in the membranes. Figure 6 shows the radial distribution functions (RDFs) between CO_2 and atoms in PIM-1. The cyano groups (ct and nt atoms), as well as the oxygen atoms (oc), have the strongest interactions with CO_2. This confirms that the cyano groups are the favourable sites in PIM-1 for sorption. Figure 7 shows the interaction energy distribution of a single CO_2 molecule in PIM-1 and PIM-7. As can be seen, the energy in PIM-1 is larger (more negative) than in PIM-7, which implies that CO_2 interacts with PIM-1 more strongly than with PIM-7.

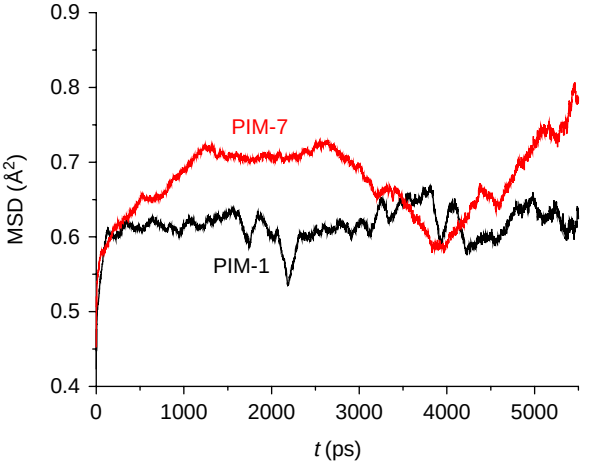

Figure 5. MSDs of polymer chains in PIM-1 and PIM-7.

Table 2. Simulated and experimental solubility coefficients [cm^3 (STP)/cm^3 (polymer) bar] and diffusion coefficients [10^{-8} cm^2/s] in PIM-1 and PIM-7 at 300 K. The experimental pressure was approximately 200 mbar [22].

	Gas	$S_{sim.}$	$S_{exp.}$ [22]	$D_{sim.}$	$D_{exp.}$ [22]
PIM-1	H_2	0.46 ± 0.03	0.58	6630 ± 215	1700
	O_2	4.11 ± 0.58	3.5	452 ± 81	81
	CO_2	50.7 ± 9	66.9	151 ± 47	26
	CH_4	14.2 ± 3.1	13.7	112 ± 27	6.8
PIM-7	H_2	0.44 ± 0.01	0.61	6860 ± 689	1100
	O_2	4.01 ± 0.26	2.35	346 ± 100	62
	CO_2	50.6 ± 5	39.5	130 ± 13	21
	CH_4	15.5 ± 3.1	9.1	60 ± 6	5.1

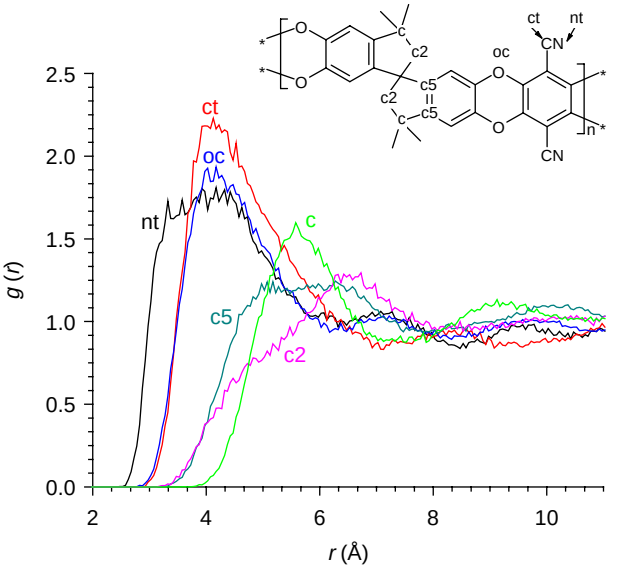

Figure 6. RDFs between CO_2 and atoms in PIM-1.

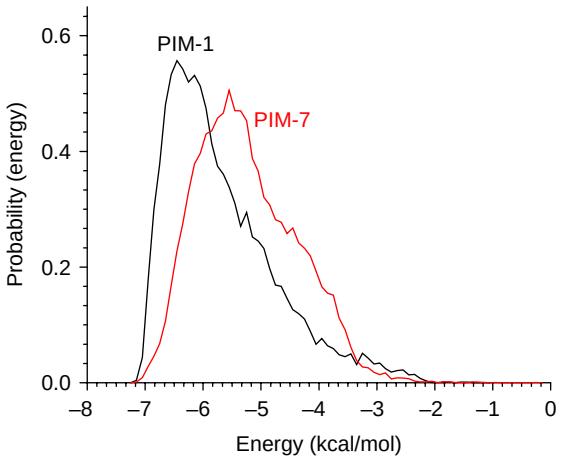

Figure 7. Energy distribution of a single CO_2 molecule in PIM-1 and PIM-7.

In the two membranes, the solubility coefficients increase in the order of $H_2 < O_2 < CH_4 < CO_2$. This reveals that the membranes have the largest affinity for CO_2 and the least for H_2. It is commonly recognised that the solubility coefficients can be correlated with the critical temperature T_c of sorbate [48]:

$$\ln S = \ln S_0 + K_c T_c, \tag{8}$$

where S_0 and K_c are constants; specifically K_c is independent of the chemical structure of the polymer membrane. The critical temperatures of the four gases are given in Table 3. Reasonably good correlations are found in Figure 8 between the calculated semi-logarithmic solubility coefficients and critical temperatures. We note that T_c is the signature of condensability and a gas with higher T_c has a stronger interaction with the membrane and therefore a larger solubility.

3.3 *Diffusion*

The underlying mechanism of gas diffusion in a polymer membrane is regarded as an activated process. A molecule is trapped in a void for a certain amount of time and then crosses the energy barrier to jump into a neighbouring void. The frequency of jumping depends on how large the energy barrier is, which in turn is governed by the specific polymer membrane and gas molecule. This process continues repeatedly as a result of the opening and closing of voids in the polymer matrix. Figure 9 shows the representative displacement of a single gas molecule as a function of time within 8 ns simulation duration in PIM-7. A similar behaviour was observed in PIM-1 and is not shown here. In general, three types of motions are observed in Figure 9 for different gases. The first type is for the H_2 molecule, which is seldom trapped because of its small diameter and frequent jumping. The second type is for the O_2 or CO_2 molecule, which is trapped in a void for 2–4 ns and then jumps to another void. As illustrated for O_2, in the first 4 ns, the molecule is trapped and oscillates with a maximum magnitude of 8–8.5 Å. This is consistent with the largest void in the PIM-7 membrane shown in Figure 4. At the subsequent duration, the molecule jumps to the adjacent void. The third type is for the CH_4 molecule with a significant trapped motion. This is because CH_4 is relatively larger in diameter and does not readily jump into another void. As a consequence, H_2 moves the fastest and CH_4 moves the slowest.

Table 3. Critical temperatures, kinetic diameters d_k, collision diameters d_c and effective diameters d_{eff} of H_2, O_2, CO_2 and CH_4. The diameters are in Å.

Gas	T_c (K)	d_k [58]	d_c[59]	d_{eff}
H_2	33.2	2.89	2.83	2.85
O_2	154.6	3.46	3.47	3.46
CO_2	304.2	3.30	3.94	3.61
CH_4	190.6	3.80	3.76	3.78

Gas diffusion can be described by the MSD as a function of time t as $\mathrm{MSD}(t) \propto t^{\gamma}$, where the scaling index γ is the signature of different types of diffusion. Specifically, $\gamma < 1, > 1$ and $= 1$ correspond to sub-, super- and normal diffusion, respectively. The sub-diffusion is usually observed within a short time and attributed to the structural correlation of an immediate environment that retards diffusion. The super-diffusion occurs under convective or hydrodynamic transport. The normal (also called Einstein) diffusion takes place if molecules move randomly. For the four gases in PIM-1 and PIM-7 membranes, normal diffusion was observed at sufficiently long time. Consequently, the diffusion coefficient was estimated using the Einstein relationship:

$$D = \frac{1}{6N}\frac{\mathrm{d}}{\mathrm{d}t}\lim_{t\to\infty}\sum_{k=1}^{N}\left\langle |r_k(t) - r_k(0)|^2 \right\rangle. \tag{9}$$

Table 2 lists the diffusion coefficients of four gases (H_2, O_2, CO_2 and CH_4) at 300 K. The simulation values were the averages of three independent runs with different initial configurations. The experimental diffusion coefficients in both the membranes increase in the following order: $CH_4 < CO_2 < O_2 < H_2$, which is well captured by the simulation. For a given gas, the diffusion coefficients in PIM-1 are slightly larger than in PIM-7, particularly observed in the experimental data. This is due to the cyano groups in PIM-1, which increase the *d*-spacing and FFV of PIM-1.

The simulated diffusion coefficients overestimate experimental results by approximately five-fold, except for CH_4, which is usually acceptable in the prediction of gas diffusion in polymer membranes. The deviation here is primarily attributed to the lower densities of the model membranes. As discussed above, the predicted densities are 3–4% lower than the measured values. Compared to

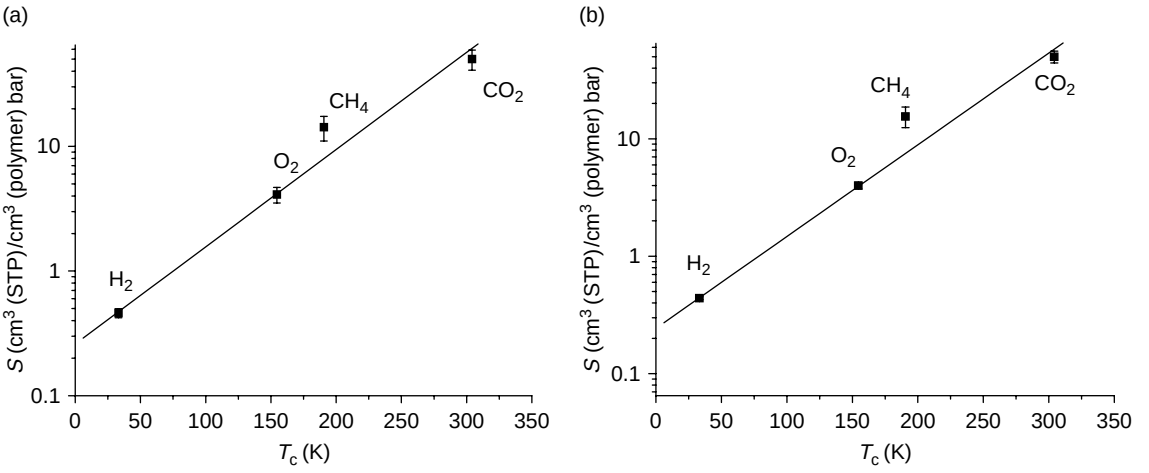

Figure 8. Simulated solubility coefficients in (a) PIM-1 and (b) PIM-7 as a function of critical temperature T_c.

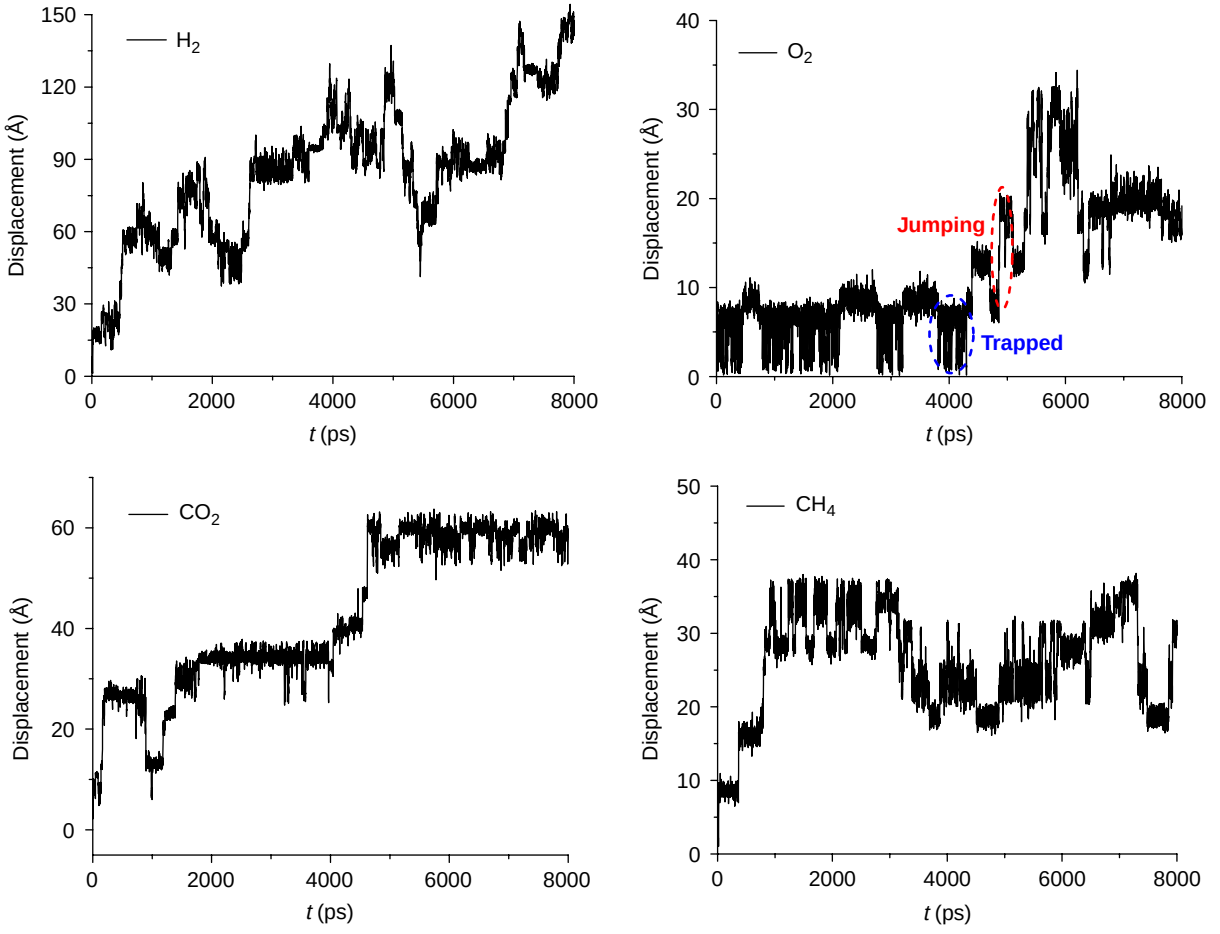

Figure 9. Representative displacement of a single gas molecule as a function of time in PIM-7. The trapped and jumping motions are schematically indicated for O_2.

experimental samples, the model membranes are a bit looser and contain a larger degree of free volume. Therefore, gas diffuses faster in the model membranes. After a closer observation, it is found that the deviation between the simulated and experimental diffusion coefficients of CH_4 is larger than other gases. This is because CH_4 has a larger molecule size and the density of the membrane exerts a greater impact on its diffusion.

In this sense, it is important to construct a model membrane with density matching closely to the experimental value. There are a number of other factors, which would cause the discrepancy of diffusion coefficients between the simulation and the experiment. For example, simulation gives the self-diffusion coefficient, whereas experiment typically reports the transport diffusion coefficient by a time-lag measurement. The self- and transport diffusion coefficients are identical only at infinite dilution, but experimental condition is usually at finite pressure/concentration. The accurate prediction of the diffusion coefficient requires not only a good force field, but also a well-equilibrated model membrane. It was found that the equilibration procedure to construct the model membrane affects gas diffusion [49]. With the 'self-avoiding' random-walk method to build the membrane, anisotropy may exist and leads to the non-uniform distribution of polymer chains. Even if the overall density is close to the experimental density, the void distribution in the model membrane may not be the same as in the true membrane. Furthermore, the polymer chain length also plays a role in gas diffusion [50]. The model built with short polymer chains has a larger FFV than the model with long polymer chains. Consequently, the diffusion coefficient predicted in the former is greater than in the latter. For PIM-1, the weight-average molar mass was determined experimentally as 37,000 g/mol [23], which means the degree of polymerisation of PIM-1 is 797. However, in our simulation, the PIM-1 model had 15 monomers and this would lead to a faster diffusion than experimentally measured. In addition, the short polymer chains have a greater mobility, which in turn facilitates diffusion.

It is instructive to compare gas diffusion in PIM-1 and PIM-7 with that in other polymers and porous structures. As a result of the microporous feature, the two PIMs have diffusion coefficients larger than most glassy polymers, though smaller than extremely permeable poly[1-(trimethylsilyl)-1-propyne], poly(4-methyl-2-pentyne) and Teflon AF [22]. In contrast, the diffusion coefficients in the two PIMs are two to three orders of magnitude lower than in silicalite and MOFs [51–53]. This is because the pores/voids are irregular in amorphous PIMs, but well defined and highly ordered in silicalite and MOFs.

Several studies have proposed a correlation between the diffusion coefficient and the diameter [54–56]. For the four gas molecules in this study, Table 3 lists the kinetic diameter d_k related to the molecular sieve dimension, the LJ collision diameter d_c related to the intermolecular separation distance and the effective diameter $d_{eff} = \sqrt{d_c d_k}$. Figure 10 shows the correlations of the semi-logarithmic diffusion coefficients with d_k and d_c. In general, the correlations are good except for CO_2, which is a linear molecule and cannot be described well by either d_k or d_c. To improve the correlations particularly for CO_2, the effective diameter d_{eff} is used instead. As shown in Figure 11, the correlations are better with the effective diameter for all the four gases in both membranes, which can be described by the Teplyakov–Meares equation [57]:

$$\log D = K_1 - K_2 d_{eff}^2, \tag{10}$$

where K_1 and K_2 are constants only depending on the intrinsic properties of membranes. With the molecular-based correlations, the diffusion coefficients of other gases can be predicted.

3.4 *Permeation*

Based on the solution–diffusion mechanism, permeability in a polymer membrane can be expressed by $P = S \cdot D$. The separation factor between two species i and j in a membrane is usually evaluated by the ideal permeability selectivity:

$$\alpha_{i/j} = \frac{P_i}{P_j} = \frac{S_i}{S_j}\frac{D_i}{D_j}, \tag{11}$$

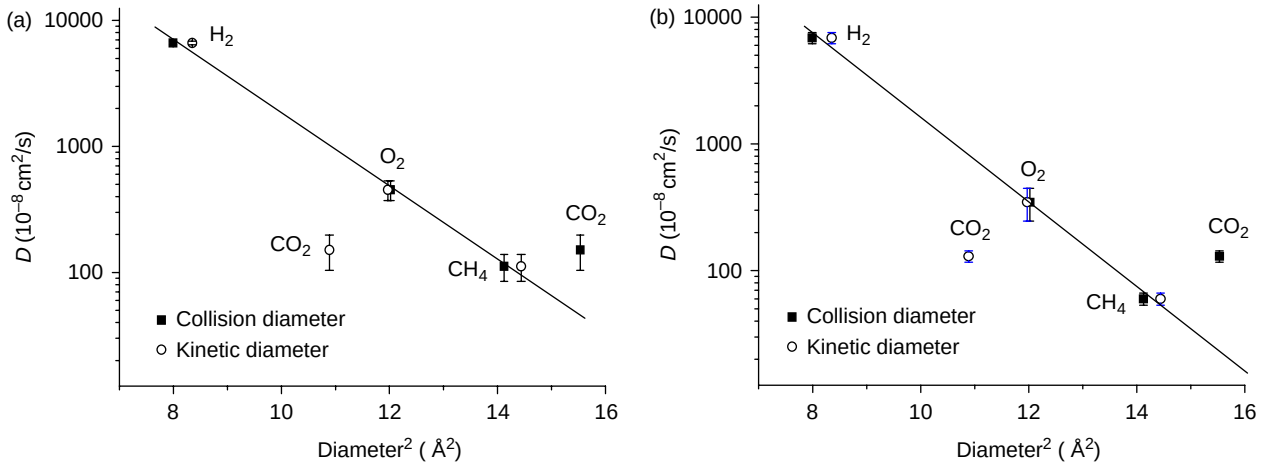

Figure 10. Simulated diffusion coefficients in (a) PIM-1 and (b) PIM-7 as a function of squared collision and kinetic diameters.

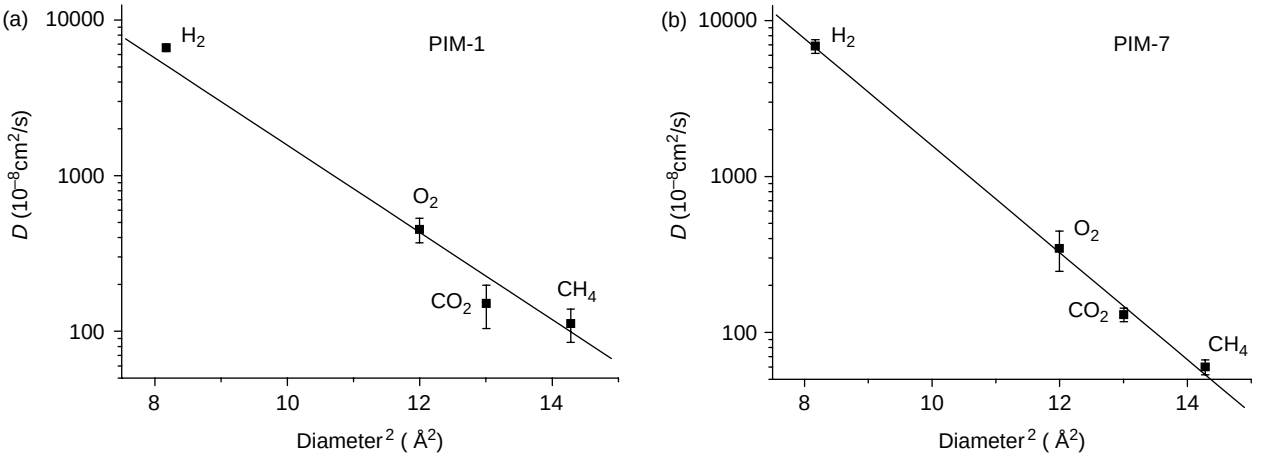

Figure 11. Simulated diffusion coefficients in (a) PIM-1 and (b) PIM-7 as a function of squared effective diameter.

Table 4. Solubility, diffusivity and permeability selectivities of CO_2 over H_2, O_2 and CH_4 in PIM-1 and PIM-7 at 300 K.

		$S_{CO_2}/S_{(i)}$		$D_{CO_2}/D_{(i)}$		$P_{CO_2}/P_{(i)}$	
	Gas	Sim.	Exp.	Sim.	Exp.	Sim.	Exp.
PIM-1	H_2	109	117	0.023	0.015	2.51	1.76
	O_2	12.2	19.1	0.33	0.32	4.03	6.11
	CH_4	3.52	4.92	1.35	3.82	4.75	18.8
PIM-7	H_2	113	64.8	0.019	0.019	2.15	1.23
	O_2	12.5	16.8	0.37	0.34	4.63	5.71
	CH_4	3.23	4.35	2.17	4.12	7.01	17.9

where S_i/S_j is the solubility selectivity and D_i/D_j is the diffusivity selectivity. Table 4 gives the solubility, diffusivity and permeability selectivities for CO_2 over H_2, O_2 and CH_4 in PIM-1 and PIM-7 membranes. It should be noted that the separations of CO_2/H_2, CO_2/O_2 and CO_2/CH_4 are practically important for H_2 production, food packaging and natural gas purification. The simulated solubility selectivities match well with the experimental values. The diffusivity and permeability selectivities are also close to the experimental values except for CO_2/CH_4. The reason, as mentioned earlier, is that the simulated diffusion coefficient of CH_4 is larger than the experimental result. CO_2 is more permeable in PIM-1 and PIM-7 compared to the other three gases, and the solubility selectivity dominates the overall permeability selectivity. As demonstrated experimentally, PIM-1 and PIM-7 exhibit not only high solubility and diffusion coefficients, but also high selectivity, and surpass the Robeson's upper bound [24].

4. Conclusions

Molecular simulations have been conducted to investigate the permeation of four gases (H_2, O_2, CH_4 and CO_2) in PIM-1 and PIM-7 membranes. The PIMs have rigid contorted structures with the FFV of 47.7 and 46.6%, substantially larger than in common glassy polyimides. A wide range of interconnected voids with a diameter up to 9 Å exist in the membranes. The predicted densities are close to the experimentally determined data. The solubility parameters of both membranes are very close, implying that the interactions in PIM-1 and PIM-7 are similar due to their largely similar chain structures. In the presence of cyano groups, PIM-1 possesses a lower density and a larger FFV than PIM-7.

PIM-1 and PIM-7 have the largest affinity for CO_2 and the least for H_2. The solubility coefficients of the four gases increase in the following order: $H_2 < O_2 < CH_4 < CO_2$. Good agreement was observed between the simulation and the experiment. As a consequence of the microporous structure and polar sites, the solubility coefficients in PIM-1 and PIM-7 are substantially higher than in other polymers. The solubility coefficients correlate well with the critical temperatures of gases. The cyano groups in PIM-1 enhance the affinity for gas, and PIM-1 thus exhibits a larger solubility coefficient than PIM-7.

The activated diffusion processes in PIM-1 and PIM-7 were identified by the time evolution of molecular displacement. H_2 exhibits frequent jumping because of its small diameter, O_2 and CO_2 are trapped in a void for a while and then jump. With a relatively large molecule, CH_4 is predominantly trapped. Normal diffusion was observed for the four gases and the diffusion coefficients were estimated by Einstein's relation. The diffusion coefficients increase in the following order: $CH_4 < CO_2 < O_2 < H_2$. The simulated diffusion coefficients overestimate the experimental values, as the model membranes have 3–4% lower densities compared to real samples. Therefore, improved models are desirable to achieve better predictions. Because of the microporous nature, the two PIMs show larger diffusion coefficients than do most glassy polymers. The diffusion coefficients correlate well with the effective diameters of gases. PIM-1

is more diffusive than PIM-7 as the former has larger *d*-spacing and FFV. The simulated solubility, diffusivity and permeability selectivities generally match well with the experimental data. The overall permeability selectivities of three gas pairs CO_2/H_2, CO_2/O_2 and CO_2/CH_4 are dominated by the solubility selectivities. PIM-1 and PIM-7 membranes show high permeabilities and selectivities. With the intrinsic porosity and microporous character, the PIMs are attractive for gas separation.

Acknowledgements

The authors are grateful to Prof P.M. Budd for providing the experimental density value of the PIM-7 membrane and the National Research Foundation of Singapore on the Competitive Research Programme (R-279-000-261-281) for financial support.

References

[1] G. Maier, *Gas separation with polymer membranes*, Angew. Chem. Int. Ed. 37 (1998), pp. 2960–2974.
[2] R.W. Baker, *Future directions of membrane gas separation technology*, Ind. Eng. Chem. Res. 41 (2002), pp. 1393–1411.
[3] N.W. Ockwig and T.M. Nenoff, *Membranes for hydrogen separation*, Chem. Rev. 107 (2007), pp. 4078–4110.
[4] L. Shao, B.T. Low, T.-S. Chung, and A.R. Greenberg, *Polymeric membranes for the hydrogen economy: Contemporary approaches and prospects for the future*, J. Membr. Sci. 327 (2009), pp. 18–31.
[5] P. Bernardo, E. Drioli, and G. Golemme, *Membrane gas separation: A review/state of the art*, Ind. Eng. Chem. Res. 48 (2009), pp. 4638–4663.
[6] Y. Xiao, T.-S. Chung, H.M. Guan, and M.D. Guiver, *Synthesis, cross-linking and carbonization of co-polyimides containing internal acetylene units for gas separation*, J. Membr. Sci. 302 (2007), pp. 254–264.
[7] B.T. Low, T.S. Chung, H. Chen, Y.-C. Jean, and K.P. Pramoda, *Tuning the free volume cavities of polyimide membranes via the construction of pseudo-interpenetrating networks for enhanced gas separation performance*, Macromolecules 42 (2009), pp. 7042–7054.
[8] X. Hu, H. Cong, Y. Shen, and M. Radosz, *Nanocomposite membranes for co$_2$ separations: Silica/brominated poly(phenylene oxide)*, Ind. Eng. Chem. Res. 46 (2007), pp. 1547–1551.
[9] C.U.P. Ribeiro and B.D. Freeman, *Sorption, dilation, and partial molar volumes of carbon dioxide and ethane in cross-linked poly(ethylene oxide)*, Macromolecules 41 (2008), pp. 9458–9468.
[10] W. Yave, A. Car, S.S. Funari, S.P. Nunes, and K.-V. Peinemann, *CO_2-philic polymer membrane with extremely high separation performance*, Macromolecules 43 (2009), pp. 326–333.
[11] J.R. Fried, M. Sadat-Akhavi, and J.E. Mark, *Molecular simulation of gas permeability: Poly(2,6-dimethyl-1,4-phenylene oxide)*, J. Membr. Sci. 149 (1998), pp. 115–126.
[12] R. Abou-Hussein, S. Wu, L. Zhang, and J.E. Mark, *Effects of some structural features of poly(dimethylsiloxane) on its unusually high gas permeabilities*, J. Inorg. Organomet. Polym. Mater 18 (2008), pp. 100–103.
[13] M. Heuchel, D. Hofmann, and P. Pullumbi, *Molecular modeling of small-molecule permeation in polyimides and its correlation to free-volume distributions*, Macromolecules 37 (2004), pp. 201–214.
[14] M. Heuchel, M. Böhning, O. Hölck, M.R. Siegert, and D. Hofmann, *Atomistic packing models for experimentally investigated swelling states induced by CO_2 in glassy polysulfone and poly(ether sulfone)*, J. Polym. Sci. B Polym.: Phys. 44 (2006), pp. 1874–1897.
[15] N.C. Karayiannis, V.G. Mavrantzas, and D.N. Theodorou, *Detailed atomistic simulation of the segmental dynamics and barrier properties of amorphous poly(ethylene terephthalate) and poly(ethylene isophthalate)*, Macromolecules 37 (2004), pp. 2978–2995.
[16] T. Spyriouni, G.C. Boulougouris, and D.N. Theodorou, *Prediction of sorption of CO_2 in glassy atactic polystyrene at elevated pressures through a new computational scheme*, Macromolecules 42 (2009), pp. 1759–1769.
[17] S. Neyertz, A. Douanne, and D. Brown, *Effect of interfacial structure on permeation properties of glassy polymers*, Macromolecules 38 (2005), pp. 10286–10298.
[18] S. Neyertz and D. Brown, *Molecular dynamics simulations of oxygen transport through a fully atomistic polyimide membrane*, Macromolecules 41 (2008), pp. 2711–2721.
[19] P.M. Budd, B. Ghanem, K. Msayib, N.B. McKeown, and C. Tattershall, *A nanoporous network polymer derived from hexaazatrinaphthylene with potential as an adsorbent and catalyst support*, J. Mater. Chem. 13 (2003), pp. 2721–2726.
[20] N.B. McKeown, P.M. Budd, K.J. Msayib, B.S. Ghanem, H.J. Kingston, C.E. Tattershall, S. Makhseed, K.J. Reynolds, and D. Fritsch, *Polymers of intrinsic microporosity: Bridging the void between microporous and polymeric materials*, Chem. Eur. J. 11 (2005), pp. 2610–2620.
[21] N.B. McKeown and P.M. Budd, *Polymers of intrinsic microporosity: Organic materials for membrane separations, heterogeneous catalysis and hydrogen storage*, Chem. Soc. Rev. 35 (2006), pp. 675–683.
[22] P.M. Budd, K.J. Msayib, C.E. Tattershall, B.S. Ghanem, K.J. Reynolds, N.B. McKeown, and D. Fritsch, *Gas separation membranes from polymers of intrinsic microporosity*, J. Membr. Sci. 251 (2005), pp. 263–269.
[23] P.M. Budd, N.B. McKeown, B.S. Ghanem, K.J. Msayib, D. Fritsch, L. Starannikova, N. Belov, O. Sanfirova, Y. Yampolskii, and V. Shantarovich, *Gas permeation parameters and other physicochemical properties of a polymer of intrinsic microporosity: Polybenzodioxane PIM-1*, J. Membr. Sci. 325 (2008), pp. 851–860.
[24] L.M. Robeson, *Correlation of separation factor vs. permeability for polymeric membranes*, J. Membr. Sci. 62 (1991), pp. 165–185.
[25] J. Ahn, W.-J. Chung, I. Pinnau, J. Song, N. Du, G.P. Robertson, and M.D. Guiver, *Gas transport behavior of mixed-matrix membranes composed of silica nanoparticles in a polymer of intrinsic microporosity (PIM-1)*, J. Membr. Sci. 346 (2010), pp. 280–287.
[26] N. Du, G.P. Robertson, J. Song, I. Pinnau, and M.D. Guiver, *High-performance carboxylated polymers of intrinsic microporosity with tunable gas transport properties*, Macromolecules 42 (2009), pp. 6038–6043.
[27] N. Du, G.P. Robertson, J. Song, I. Pinnau, S. Thomas, and M.D. Guiver, *Polymers of intrinsic microporosity containing trifluoromethyl and phenylsulfone groups as materials for membrane gas separation*, Macromolecules 41 (2008), pp. 9656–9662.
[28] N. Du, G.P. Robertson, I. Pinnau, and M.D. Guiver, *Polymers of intrinsic microporosity derived from novel disulfone-based monomers*, Macromolecules 42 (2009), pp. 6023–6030.
[29] B.S. Ghanem, N.B. McKeown, P.M. Budd, J.D. Selbie, and D. Fritsch, *High-performance membranes from polyimides with intrinsic microporosity*, Adv. Mater. 20 (2008), pp. 2766–2771.
[30] M. Heuchel, D. Fritsch, P.M. Budd, N.B. McKeown, and D. Hofmann, *Atomistic packing model and free volume distribution of a polymer with intrinsic microporosity*, J. Membr. Sci. 318 (2008), pp. 84–99.
[31] D.N. Theodorou and U.W. Suter, *Detailed molecular structure of a vinyl polymer glass*, Macromolecules 18 (1985), pp. 1467–1478.
[32] W. Smith and T.R. Forester, *DL_POLY 2.0: A general-purpose parallel molecular dynamics simulation package*, J. Mol. Graph. 14 (1996), pp. 136–141.
[33] W. Smith, C.W. Yong, and P.M. Rodger, *DL_POLY: Application to molecular simulation*, Mol. Simul. 28 (2002), pp. 385–471.
[34] H. Sun, Ab-initio *calculations and force-field development for computer-simulation of polysilanes*, Macromolecules 28 (1995), pp. 701–712.
[35] H. Sun, S.J. Mumby, J.R. Maple, and A.T. Hagler, *An* ab-initio *cff93 all-atom force-field for polycarbonates*, J. Am. Chem. Soc. 116 (1994), pp. 2978–2987.
[36] H. Sun, S.J. Mumby, J.R. Maple, and A.T. Hagler, Ab initio *calculations on small molecule analogues of polycarbonates*, J. Phys. Chem. 99 (1995), pp. 5873–5882.

[37] H. Sun and D. Rigby, *Polysiloxanes:* Ab initio *force field and structural, conformational and thermophysical properties*, Spectrochim. Acta A: Mol. Biomol. Spectrosc. 53 (1997), pp. 1301–1323.
[38] H.J.C. Berendsen, J.P.M. Postma, W.F. Vangunsteren, A. Dinola, and J.R. Haak, *Molecular-dynamics with coupling to an external bath*, J. Chem. Phys. 81 (1984), pp. 3684–3690.
[39] B. Nagasaka, T. Eguchi, H. Nakayama, N. Nakamura, and Y. Ito, *Positron annihilation and ^{129}Xe NMR studies of free volume in polymers*, Radiat. Phys. Chem. 58 (2000), pp. 581–585.
[40] S. Ban and T.J.H. Vlugt, *Zeolite microporosity studied by molecular simulation*, Mol. Simul. 35 (2008), pp. 1105–1115.
[41] S. Bhattacharya and K.E. Gubbins, *Fast method for computing pore size distributions of model materials*, Langmuir 22 (2006), pp. 7726–7731.
[42] B. Widom, *Some topics in theory of fluids*, J. Chem. Phys. 39 (1963), pp. 2808–2812.
[43] P.M. Budd, *personal communication*.
[44] R. Babarao and J.W. Jiang, *Molecular screening of metal-organic frameworks for CO_2 storage*, Langmuir 24 (2008), pp. 6270–6278.
[45] R. Babarao and J.W. Jiang, *Exceptionally high CO_2 storage in covalent-organic frameworks: Atomistic simulation study*, Energy Environ. Sci. 1 (2008), pp. 139–143.
[46] O.M. Yaghi, M. O'Keeffe, N.W. Ockwig, H.K. Chae, M. Eddaoudi, and J. Kim, *Reticular synthesis and the design of new materials*, Nature (London) 423 (2003), pp. 705–714.
[47] H.M. El-Kaderi, J.R. Hunt, J.L. Mendoza-Cortes, A.P. Cote, R.E. Taylor, M. O'Keeffe, and O.M. Yaghi, *Designed synthesis of 3D covalent organic frameworks*, Science 316 (2007), pp. 268–272.
[48] J.J. Shieh and T.S. Chung, *Gas permeability, diffusivity, and solubility of poly(4-vinylpyridine) film*, J. Polym. Sci. B: Polym. Phys. 37 (1999), pp. 2851–2861.
[49] M. Meunier, *Diffusion coefficients of small gas molecules in amorphous cis-1,4-polybutadiene estimated by molecular dynamics simulations*, J. Chem. Phys. 123 (2005), pp. 1–7.
[50] P. Gestoso and M. Meunier, *Barrier properties of small gas molecules in amorphous cis-1,4-polybutadiene estimated by simulation*, Mol. Simul. 34 (2008), pp. 1135–1141.
[51] L. Sarkisov, T. Duren, and R. Snurr, *Molecular modelling of adsorption in novel nanoporous metal-organic materials*, Mol. Phys. 102 (2004), pp. 211–221.
[52] A.I. Skoulidas and D. Sholl, *Self-diffusion and transport diffusion of light gases in metal-organic framework self-diffusion and transport diffusion of light gases in metal-organic framework*, J. Phys. Chem. B 109 (2005), pp. 15760–15768.
[53] R. Babarao and J.W. Jiang, *Diffusion and separation of CO_2 and CH_4 in silicalite, C_{168} schwarzite, and irmof-1: A comparative study from molecular dynamics simulation*, Langmuir 24 (2008), pp. 5474–5484.
[54] V.P. Shantarovich, I.B. Kevdina, Y.P. Yampolskii, and A.Y. Alentiev, *Positron annihilation lifetime study of high and low free volume glassy polymers: Effects of free volume sizes on the permeability and permselectivity*, Macromolecules 33 (2000), pp. 7453–7466.
[55] H. Lin and B.D. Freeman, *Gas solubility, diffusivity and permeability in poly(ethylene oxide)*, J. Membr. Sci. 239 (2004), pp. 105–117.
[56] T.C. Merkel, V.I. Bondar, K. Nagai, B.D. Freeman, and I. Pinnau, *Gas sorption, diffusion, and permeation in poly(dimethylsiloxane)*, J. Polym. Sci. B: Polym. Phys. 38 (2000), pp. 415–434.
[57] V. Teplyakov and P. Meares, *Correlation aspects of the selective gas permeabilities of polymeric materials and membranes*, Gas Sep. Purif. 4 (1990), pp. 66–74.
[58] D.W. Breck, *Zeolite Molecular Sieves: Structure, Chemistry and Use*, John Wiley & Sons, Inc., New York, 1974.
[59] B.E. Poling, J.M. Prausnitz, and J.P. O'Connell, *The Properties of Gases and Liquids*, 5th ed., McGraw-Hill, New York, 2000.